ELSEVIER

Ceramics International 31 (2004) 197–204

CERAMICS INTERNATIONAL

www.elsevier.com/locate/ceramint

R-curve behavior of Si_3N_4 whisker-reinforced Si_3N_4 matrix composites

Lin-Hua Zou[a,b,*], Yong Huang[a], Dong-Soo Park[b], Byung-Uk Cho[b], Hai-Doo Kim[b], Byung-Dong Han[b]

[a] *State Key Laboratory of New Ceramics and Fine Processing, Tsinghua University, Beijing 100084, PR China*
[b] *Ceramic Materials Group, Korea Institute of Machinery & Materials, 66 Sang-Nam-Dong, Chang-Won City, Kyung-Nam 641-010, South Korea*

Received 8 July 2003; received in revised form 2 March 2004; accepted 23 April 2004

Abstract

Three kinds of β-Si_3N_4 whisker-reinforced Si_3N_4 composites with different degree of whisker alignment were prepared by using tape casting, extrusion and hot pressing processes. Among these composites, one is obtained from a laminate with tapes, another is from a laminate stacked alternatively with tapes and extruded wires, and the last one is closely stacked with wires. The same whisker orientation was followed with all the tapes or wires. Four-point bending tests by stepped loading were employed to determine R-curves for the three materials. The results show that all the materials have better R-curve behaviors than composites with randomly oriented whiskers. The fracture toughness of the three materials are, respectively, 11.18, 11.44 and 10.60 MPa $m^{1/2}$, and the corresponding threshold values for stable crack propagation are 9.14, 10.92 and 9.32 MPa $m^{1/2}$, respectively.

Keywords: B. Composites; D. Si_3N_4; R-curve behavior; Whisker alignment

1. Introduction

During a few past decades, research on toughening of silicon nitride has progressed considerably, particularly with regard to the whisker reinforcing method. Since Faber and Evans [1] put forward the toughening mechanism of crack deflection in composites, Becher [2] discussed the model of toughening by crack-bridging processes, and described the behavior observed in whisker-reinforced ceramics: this gives an alternative way to improve fracture resistance by microstructure design. In view of improving fracture toughness, much work has been done to align the whisker orientation and increase the number of aligned whiskers, capable of interacting with planar cracks normal to their orientation [3–7].

Due to the mechanisms of crack deflection and bridging, crack propagation requires an additional energy for long grain debonding and pull-out in order to overcome the tractions of grain bridging. This will result in a rising-crack-growth-resistance behavior, i.e. R-curve behavior. Even in some monolithic ceramics and in composites with whisker randomly orientated, the materials show good R-curve behavior, such as in situ reinforced silicon nitrides [8–11], alumina [8,12], silicon carbides [13], silicon carbide whisker-reinforced alumina composites [14], silicon nitride–titanium nitride composites [15], etc. So the β-Si_3N_4 whisker-reinforced Si_3N_4 matrix composites with whisker alignment can be expected to have better R-curve behavior, as proved by Ohji et al. [16], who prepared the material with whisker alignment by using tape casting processing. However, further studies on measurement of R-curve behavior for this kind of material are still lacking.

The measurement of R-curve behavior is commonly based on the indentation-strength (I-S) method, which was first outlined by Krause Jr. [12] and widely used [13–16]. However, because the empirical power-law equa-

* Corresponding author.
E-mail address: linhua_zou@hotmail.com (L.-H. Zou).

0272-8842/$30.00
doi:10.1016/j.ceramint.2004.04.013

tion describing crack-size dependence of toughness was assumed a priori in this method, which cannot be always physically the most appropriate, the parameters of the equation were only assessed from the indentation load dependence of strength. Ramachandran et al. [8] demonstrated that R-curves for toughened ceramics could be evaluated by measurements of lengths of cracks originating at controlled indentation flaws, and the following empirical equation could well fit the measured R-curve data:

$$K_R(c) = K_\infty - (K_\infty - K_0)\exp\left(-\frac{c}{\lambda}\right) \quad (1)$$

where K_∞ and K_0 are upper-bound and lower-bound fracture toughness at large and small crack length limits, respectively, c the radial crack half length, and λ a crack length normalizing length parameter.

Xi and Guan incorporated the initial indentation radial crack half length c_0 into the formula (1), and gave an improved function [17]:

$$K_R(c) = K_\infty - (K_\infty - K_0)\exp\left(-\frac{c - c_0}{\lambda}\right) \quad (2)$$

where K_0 equals $K_R(c_0)$, which can be regarded as the threshold value of fracture resistance at the start of stable crack propagation, the other parameters have the same meanings as in Eq. (1). The modified equation turned out to be more effective in fitting the R-curves smoothly.

In this paper, the improved equation is employed to describe the R-curves for three kinds of β-Si_3N_4 whisker-reinforced Si_3N_4 composites with different whisker alignment. Combined with toughening mechanisms and the difference of the processing to fabricate the materials, the experimental results were further explained.

2. Experiment procedure

2.1. Material preparation

The tapes of Si_3N_4 was prepared by tape casting a slurry containing 89 wt.% α-Si_3N_4 (SN-E10, Ube Industries Co. Ltd., Tokyo, Japan), 6 wt.% Y_2O_3 (fine, H.C. Starck Co. GmbH, Berlin, Germany), 2 wt.% Al_2O_3 (AKP30, Sumitomo Chemical Co., Osaka, Japan) and 3 wt.% β-Si_3N_4 whiskers (SN-WB, Ube Industries Ltd.). The powders without whiskers were first mixed for 4 h by planetary ball milling in the media of a solvent containing methylethylketone (MEK) and 20 vol.% ethanol, with dispersant (KD-1, ICI Chemical Co., Barcelona, Spain) added. After 4 h milling, polyvinylbutyral (PVB, Aldrich, Milwaukee, WI, USA) as binder and dibutylphthalate (DBP, Kanto Chemical Co. Inc., Tokyo, Japan) as plasticizer were added, respectively, then the planetary ball milling was resumed for 3.5 h, and finally stopped to add whiskers and resumed for 0.5 h milling. Subsequently, the slip was degassed under vacuum and then was poured into the reservoir of the Doctor blade; Doctor blade was lifted up 450 μm from the bottom. The tape was dried in open air at ambient temperature. Through controlling the viscosity of the slip, or adjusting the height of the Doctor blade from the bottom, different thickness of tapes can be obtained. Sheets of 35 mm × 35 mm size were cut from the dried tape.

The mixed powders used for extrusion have the same composition with that used for tape casting. First, the powders without whiskers were mixed for 4 h by using planetary ball milling in the media of ethanol, then whiskers were added into the jar, and ball milling was resumed for 0.5 h. Then, the mixed powders were dried by using a Büchi Rotavapor R-200, and finally sieved through a 70 mesh. The dough used for extrusion was prepared by mixing the raw mixed powders, the binder of 15 wt.% aqueous PVA, the pasticizer of glycerine, and the lubricant of paraffin by using a rolling compaction system. The obtained homogeneous dough was aged in a sealed vessel with moist environment for 24 h. Finally, the green body wires were extruded through an orifice with a diameter of 0.2 mm.

The tapes, the tapes and wires, the wires were stacked, respectively, to make three kinds of different laminates with the same whisker orientation followed, the tape and the wires were alternatively stacked, and also the wires were closely packed (Fig. 1). Three kinds of green bodies were laminated under 40 MPa and binder burnout was carried our in flowing air. Finally, the green bodies were hot pressed sintering at 2093 K for 1.5 h under 30 MPa with an atmosphere of N_2. The obtained materials with different degree of whisker alignment were designated as A, B and C, respectively.

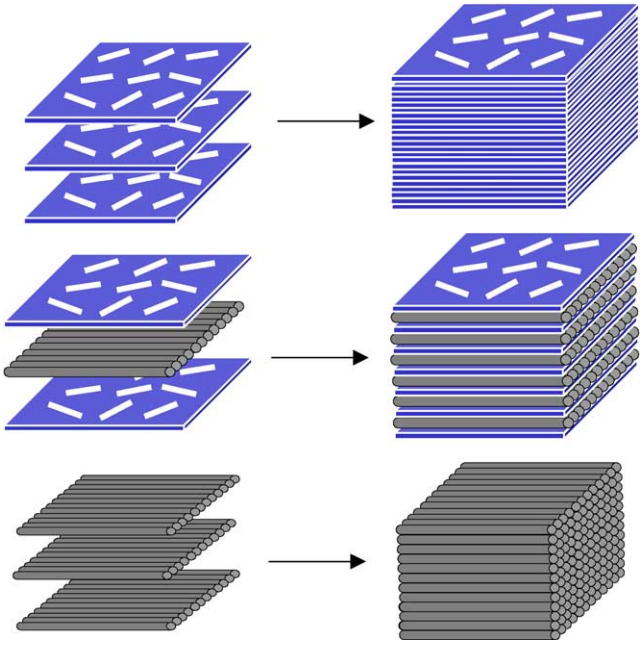

Fig. 1. The stacking processing of the green bodies for the three kinds of materials with different degrees of the whisker orientation.

2.2. Experimental method

The rectangular specimens for flexural tests were cut from the sintered billets and ground to nominal dimensions of 2.4 mm × 4.0 mm × 35 mm. The prospective tensile surface is parallel to the hot pressing plane and the surface was polished to 1 μm finish using diamond paste, the edges of the corresponding surface were slightly chamfered using a 15 μm diamond grinding disk. Then the specimens were annealed at 1273 K in nitrogen atmosphere for 1 h to eliminate the residual stresses induced by mechanical machining. Three well-developed indentations, each at least 2 mm apart, were made on the inner span (10 mm) of the prospective tensile surface of each specimen. The indentation load was 196 N. More care was taken to make sure that one of diagonal lines in each Vickers indentation and a half-penny crack were normal to the axis of the beam specimen. After the indentation, the initial radial crack length and the diagonal lengths in two orthogonal directions were measured for each indentation.

The specimens were incrementally loaded in four-point bending with an outer span of 30 mm and an inner span of 10 mm. The bending load was applied at a constant cross-head displacement speed of 0.05 mm/min on a Shimazu AG-2000A universal-testing machine. As the applied load approached a certain preset stress level, it was held for 30 s and then unloaded, the radial crack lengths for each indentation being measured by optical microscopy. Such load–unload cycles were repeated until the specimen fractured, ensuring that each specimen fractured from one of the three initial indentation-induced radial cracks.

The cross-sections of rectangular bars were characterized by XRD to analyze the degrees of whisker orientation qualitatively. The densities of the materials were measured by the Archimedes method. The indentation cracks remaining after fracture were plasma etched and then observed by SEM.

2.3. Calculations

Under this loading condition, the fracture driving force is composed of two parts, one of which from the residual stress intensity factor, according to the indentation fracture mechanics. The residual stress can be regarded as a result of a 'point force' interaction [18] that gives the following expression:

$$K_r = \chi_r \frac{P}{c^{3/2}} \tag{3}$$

where P is the indentation load (N), χ_r a parameter dependent on the indenter shape and material properties, such as Young's modulus and hardness [19]. For a crack induced by Vickers indentation, it can be expressed as [20]:

$$\chi_r = \delta \left(\frac{E}{H}\right)^{1/2} \tag{4}$$

where E is the Young's modulus, H the apparent hardness of the material, and δ a geometrical factor independent of the material (a value of $\delta = 0.018$ is used for calculations [21]). The apparent hardness is defined as the mean contact stress in the impression area [20]:

$$H = \frac{P}{2d^2} \tag{5}$$

where d is the half-diagonal length of the impression.

Another part of the fracture driving force is produced by the applied bending stress (σ_a). The corresponding stress intensity factor is determined by the following equation:

$$K_a = Y_a \sigma_a a^{1/2} \tag{6}$$

where Y_a is a dimensionless shape factor, which can be calculated basing on an empirical stress intensity factor equation for the surface crack by Newman Jr. and Raju [22], a being the crack depth (mm). The crack depth a is related to the crack length depending on the crack shape. References [23,24] show that the shape of surface indentation-induced crack changes from semicircular to semi-elliptical as it propagates under the bending stress. The shape change of the crack can be described approximately according to Li et al. [10] with the following equation:

$$\frac{a}{c} = 1.2 - 0.2\left(\frac{c}{c_0}\right) \tag{7}$$

The superposition of Eqs. (3) and (6) must equal the fracture resistance:

$$K_R = K_r + K_a = \chi_r \frac{P}{c^{3/2}} + Y_a \sigma_a a^{1/2} \tag{8}$$

For a given bending stress σ_a and a corresponding crack length c, fracture resistance K_R can be calculated through Eqs. (7) and (8).

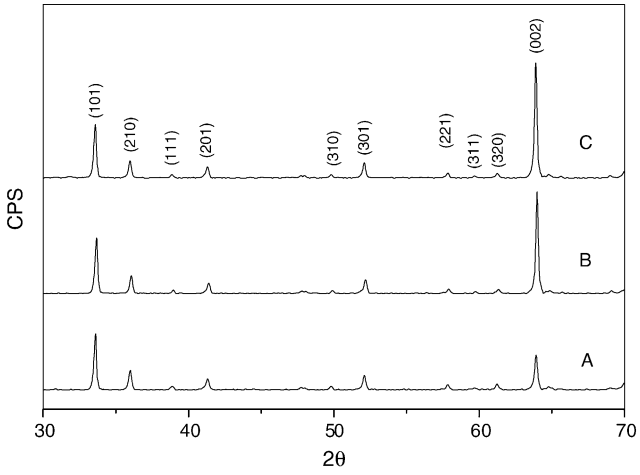

Fig. 2. The XRD patterns on the transverse planes normal to the whisker orientation for three kinds of specimens.

Table 1
The basic physical properties for the materials used for R-curve measurement

Properties	A	B	C
Young's modulus (E, GPa)	302	302	302
Apparent hardness (H, GPa)	33.17	31.06	32.42
Density (g/cm^3)	3.246	3.228	3.212
Residual stress factor (χ_r)	0.054	0.056	0.055

Stable crack extension will continue if σ_a increases to maintain the following conditions [14]:

$$\begin{cases} K_r + K_a = K_R \\ \dfrac{d(K_r + K_a)}{dc} < \dfrac{dK_R}{dc} \end{cases} \quad (9)$$

3. Results and discussion

3.1. Whisker orientation

Fig. 2 shows the X-ray diffraction patterns of the planes normal to the whisker orientation for materials A, B and C. It

Table 2
Corresponding data for R-curve of material A

c (μm)	K_R (MPa m$^{1/2}$)	σ_a (MPa)	Y_a
109	9.52	12.41	69.893
110	9.56	24.82	33.229
111	9.61	37.22	21.059
112	9.66	49.63	15.010
112	9.83	62.04	11.581
114	9.77	74.45	9.031
114	9.94	86.85	7.452
114	10.11	99.26	6.268
114	10.28	111.67	5.347
114	10.45	124.08	4.610
114	10.62	136.48	4.007
114	10.79	148.89	3.505
114	10.96	161.30	3.080
114	11.13	173.71	2.715
115	11.20	186.11	2.381
115	11.37	198.52	2.110
116	11.44	210.93	1.861
121	11.14	223.34	1.625
125	10.98	235.74	1.443
126	11.08	248.15	1.296
128	11.11	260.56	1.170
132	11.00	272.97	1.069
133	11.12	285.37	0.974
137	11.05	297.78	0.907
140	11.06	310.19	0.848
143	11.08	322.60	0.799
147	11.06	335.00	0.766
147	11.25	347.41	0.712
151	11.26	359.82	0.693
154	11.33	372.23	0.671
158	11.36	384.63	0.662
164	11.35	397.04	0.671
179	11.11	409.45	0.739
183	11.13	416.40	0.747

Table 3
Corresponding data for R-curve of material B

c (μm)	K_R (MPa m$^{1/2}$)	σ_a (MPa)	Y_a
100	11.17	12.94	82.075
104	10.71	25.88	36.814
104	10.88	38.81	23.659
104	11.05	51.75	17.081
104	11.22	64.69	13.134
107	10.97	77.63	10.021
107	11.14	90.57	8.240
107	11.32	103.50	6.904
111	10.98	116.44	5.560
111	11.15	129.38	4.785
111	11.33	142.32	4.150
113	11.27	155.25	3.545
113	11.45	168.19	3.112
115	11.40	181.13	2.695
117	11.37	194.07	2.350
119	11.35	207.01	2.062
119	11.53	219.94	1.837
122	11.43	232.88	1.622
126	11.27	245.82	1.443
128	11.29	258.76	1.298
128	11.47	271.70	1.171
130	11.51	284.63	1.063
133	11.48	297.57	0.975
137	11.41	310.51	0.908
141	11.36	323.45	0.854
144	11.38	336.38	0.805
148	11.37	349.32	0.772
152	11.37	362.26	0.746
156	11.40	375.20	0.727
159	11.48	388.14	0.706
163	11.52	401.07	0.696
170	11.49	414.01	0.709
178	11.46	426.95	0.729
193	11.30	439.89	0.784
200	11.36	452.83	0.795

Table 4
Corresponding data for R-curve of material C

c (μm)	K_R (MPa m$^{1/2}$)	σ_a (MPa)	Y_a
111	9.39	13.14	64.457
112	9.44	26.29	30.708
114	9.39	39.43	19.202
114	9.57	52.58	13.935
114	9.75	65.72	10.775
114	9.93	78.87	8.668
114	10.11	92.01	7.163
114	10.30	105.16	6.034
114	10.48	118.30	5.156
117	10.34	131.45	4.303
117	10.52	144.59	3.756
117	10.71	157.74	3.300
124	10.42	184.03	2.451
126	10.44	197.17	2.168
127	10.55	210.32	1.941
128	10.66	223.46	1.745
131	10.63	236.61	1.567
137	10.42	249.75	1.416
148	10.40	289.19	1.124
151	10.46	302.33	1.057
156	10.44	315.48	1.008

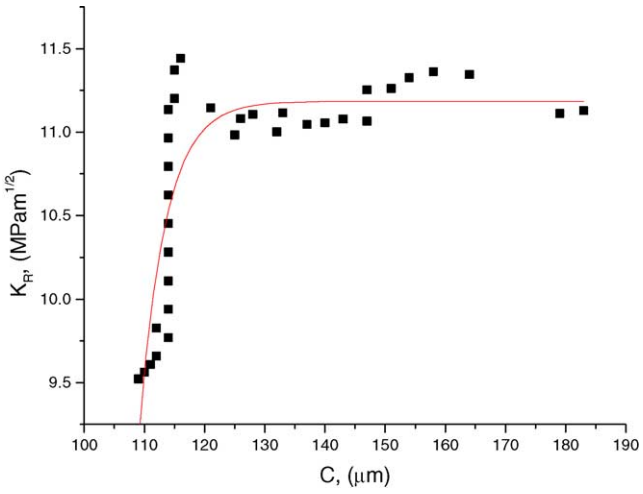

Fig. 3. R-curve behavior for the material A.

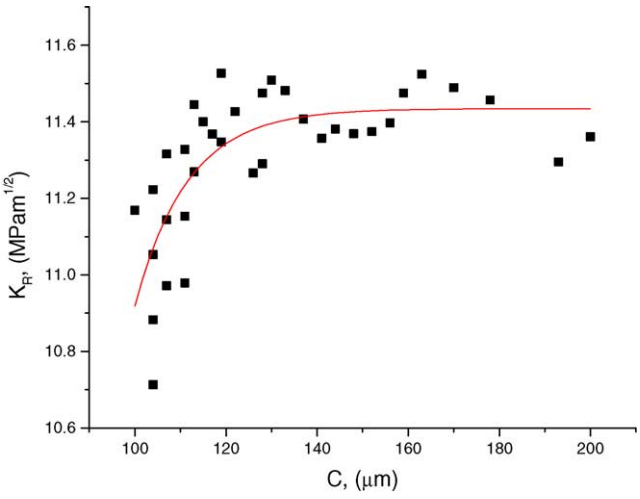

Fig. 4. R-curve behavior for the material B.

indicates that there exist distinct differences among the (0 0 2) peaks, the intensity of material A is the lowest, C is the highest, and B is intermediate. Because the β-Si_3N_4 crystal has a hexagonal structure and (0 0 2) is its basal plane, the (0 0 2) plane will be parallel to the diffracted surface if whiskers are well aligned. The results demonstrate that material C has the highest degree of whisker alignment, and it decreases following the order from material C to B and to A. This is the result as expected, as generally the degree of whisker alignment by the extrusion process is higher than that by the tape casting.

3.2. R-curve behavior

All the measurement results on basic physical properties for three kinds of materials are listed in Table 1. The Young's modulus data adopted here were measured in a previous work [25] for the materials with same composition.

From σ_a and measured c (Tables 2–4), fracture resistance K_R was calculated through Eqs. (7) and (8). Eq. (2) was adopted to fit these experimental data, and the results are given in Figs. 3–5, respectively. As expected, all of the three materials exhibit a well-defined R-curve behavior, which tends to become asymptotically flat with increasing crack length, and shows a higher threshold value corresponding with the point of the initial abrupt stable crack propagation. The parametric values of K_∞, K_0 and λ were obtained from such a fitting (Table 5). The critical fracture resistance just before the crack stable extension is corresponding with the threshold value (K_{th}), which is just equal to K_0 as c coincides with c_0 in Eq. (2). The results also verify that the improved equation can best describe the R-curves of the three materials. To facilitate the analysis, extrapolation was used here to infer some more meaningful results. Based on the condition of crack extension instability [14], i.e.

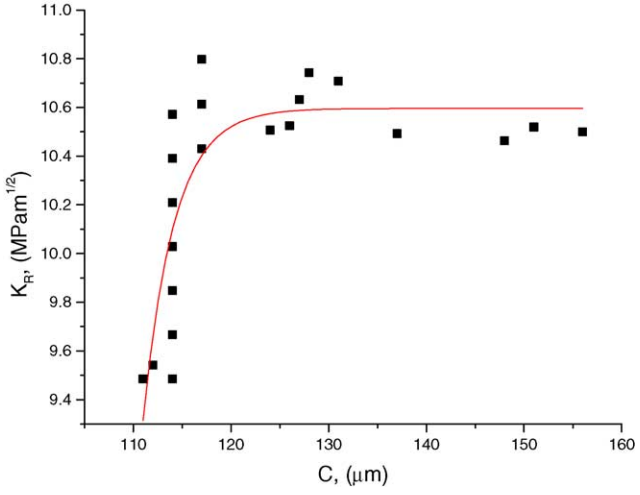

Fig. 5. R-curve behavior for the material C.

$$\begin{cases} K_r + K_a = K_R \\ \dfrac{d(K_r + K_a)}{dc} \geq \dfrac{dK_R}{dc} \end{cases} \quad (10)$$

Table 5
The exponential regression and curve extrapolation parameter values

Specimen	Regression			Extrapolation		
	K_∞ (MPa m$^{1/2}$)	K_0 (MPa m$^{1/2}$)	λ (μm)	c^* (μm)	Δc^* (μm)	K^*_{IC} (MPa m$^{1/2}$)
A	11.18	9.14	4.38	243.82	134.82	11.18
B	11.44	10.92	11.59	245.58	145.58	11.44
C	10.60	9.32	3.18	256.53	145.53	10.60

the dependence of geometry configuration factor Y_a on crack length c shows that Y_a tends to level off with increase of c (Fig. 6), so Y_a can be regarded as a constant when K_a is differentiated with respect to c. Through substitution of Eqs. (2) and (8), and assuming, approximately, $a \approx c$ during crack propagation in the extrapolation, Eq. (10)

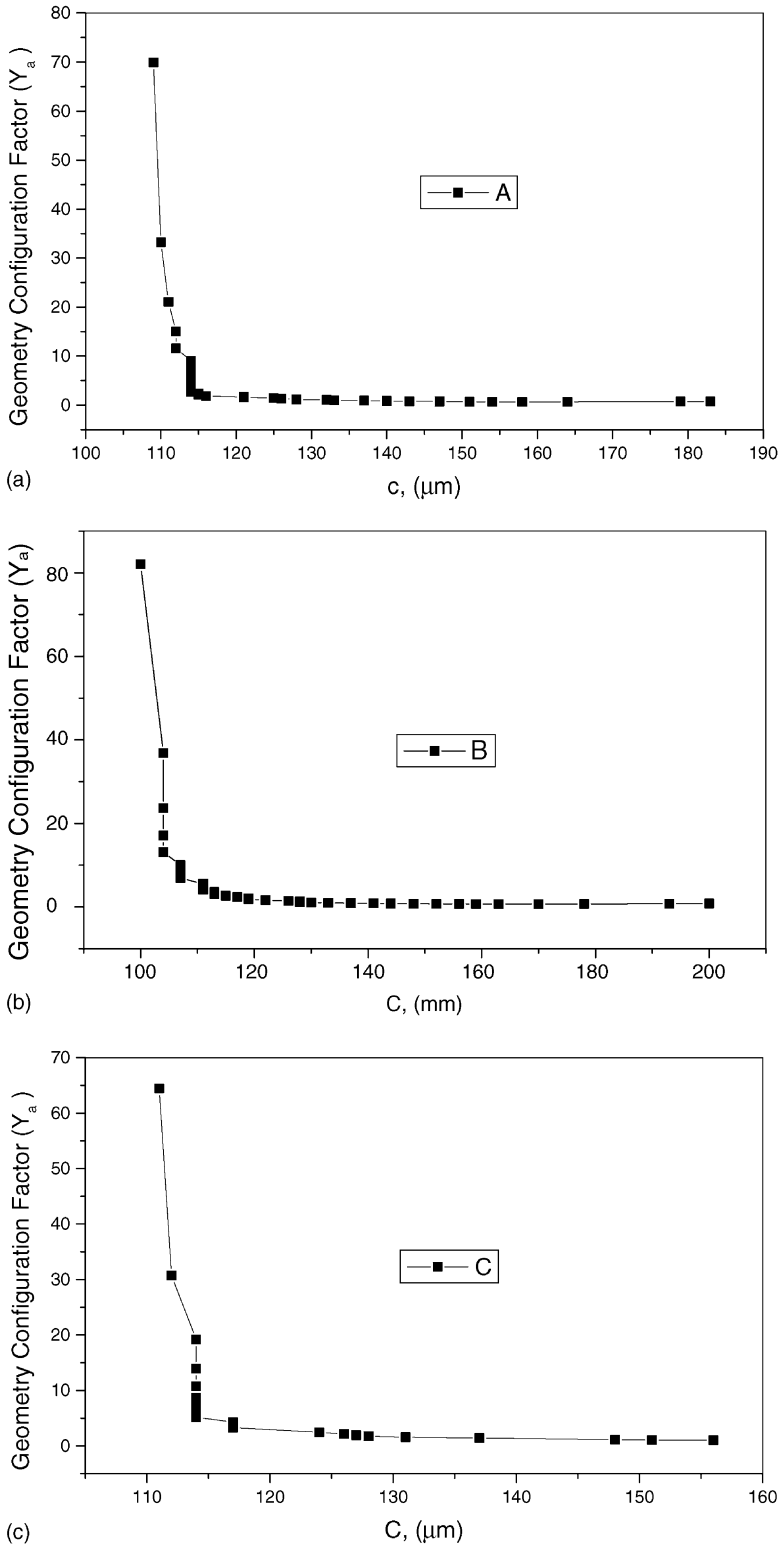

Fig. 6. The dependence of geometry configuration factor Y_a on crack length c for three materials: (a) material A; (b) material B; (c) material C.

yields:

$$\begin{cases} Y_a\sigma_a c^{1/2} + \chi_r \dfrac{P}{c^{3/2}} = K_\infty - (K_\infty - K_0)\exp\left(-\dfrac{c-c_0}{\lambda}\right) \\ \dfrac{1}{2} Y_a\sigma_a c^{-1/2} - \dfrac{3}{2}\chi_r \dfrac{P}{c^{5/2}} = \dfrac{K_\infty - K_0}{\lambda}\exp\left(-\dfrac{c-c_0}{\lambda}\right) \end{cases} \tag{11}$$

From there:

$$c = \left[\frac{K_\infty - (1+2c/\lambda)(K_\infty - K_0)\exp(-(c-c_0)/\lambda)}{4\chi_r P}\right]^{-2/3} \tag{12}$$

According to Eq. (12), progressive iteration was carried out to get the critical crack length c^*, the crack tolerance Δc^* ($c^* - c_0$) and the critical fracture toughness K^*_{IC}. The corresponding results are also shown in Table 5. It is remarkable that the critical fracture toughness coincides, for all materials, with the asymptotic fracture resistance K_∞. The values of the three materials are almost the same in magnitude. From material A to B, the fracture toughness undergoes a small increment due to the increase of whisker alignment; the threshold value increases, which means crack propagation is hard to initiate (Fig. 7a), and the critical crack length and crack tolerance increase considerably (Fig. 7b). All of these results are attributed to the better whisker alignment derived from extruded wires. However, from material B to C, the fracture toughness and threshold value decrease even if the whisker alignment increases (Fig. 7a), the critical crack length increases, while the crack tolerance is almost unchanged (Fig. 7b). Compared with A, the fracture toughness of C is a little lower, but the threshold value, the critical crack length and crack tolerance are higher than those of A (Fig. 7). It seems that an improved whisker alignment by extrusion process does not result in an expected fracture toughness increment for material C. The longest critical crack length of material C and higher crack tolerance of materials B and C are attributed to their better whisker alignment. It proves that whisker alignment is the most effective way to restrain the crack extension and improve crack tolerance. All the results indicate that the toughening effects are very remarkable by increasing the whisker alignment through tape casting and extrusion, and extrusion is more effective to increase critical crack length and crack tolerance.

In material A, due to two-dimensional distribution of whiskers, some whiskers do not orient in direction of whisker alignment. Crack deflection is inclined to occur among these whiskers when crack tip approaches to the interface of whisker and matrix. In this case, both the crack deflection and bridging mechanisms contribute to improvement of fracture toughness (Fig. 8a). However, in material C,

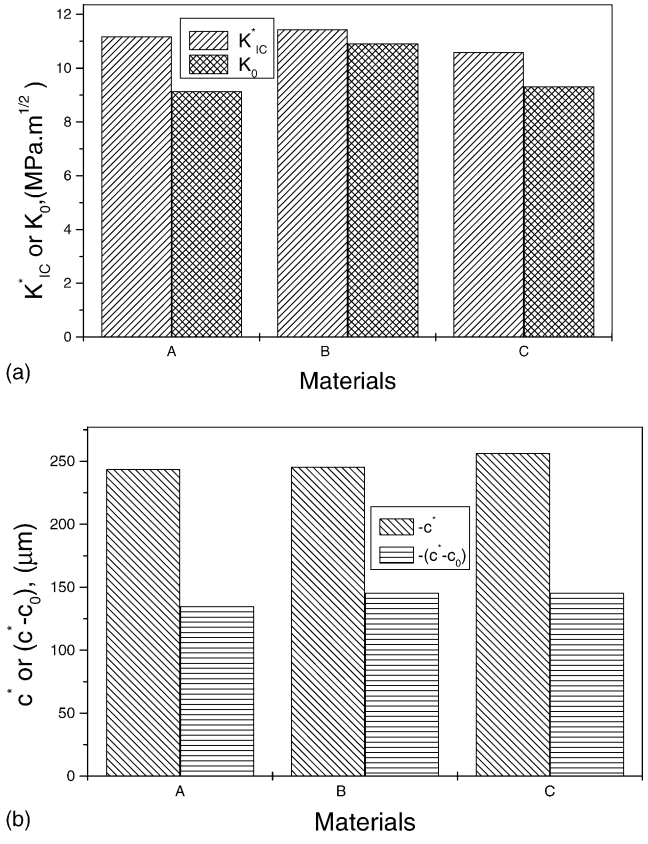

Fig. 7. The comparison of curve extrapolation parameter values for three kinds of materials: (a) fracture toughness and threshold value; (b) critical crack length and crack tolerance.

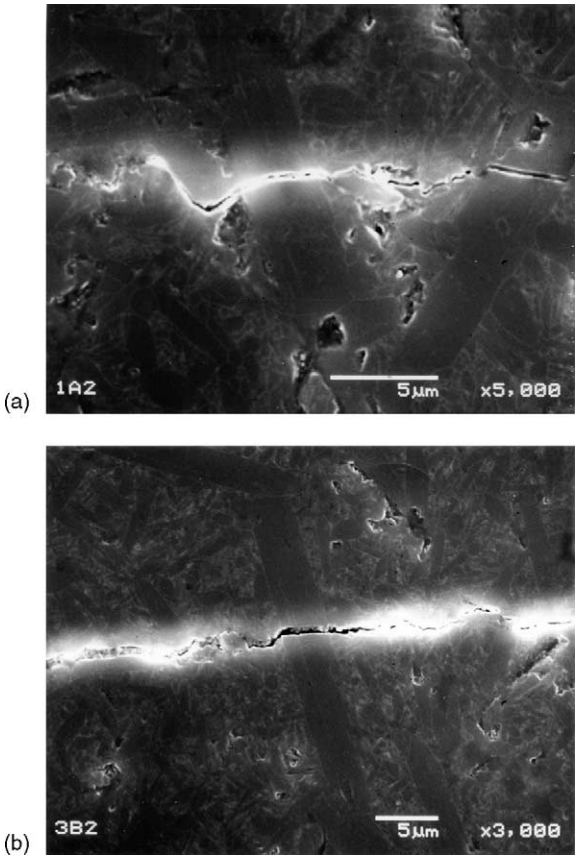

Fig. 8. The SEM micrographs of the indentation crack path after the R-curve measurement: (a) material A; (b) material C.

because more whisker alignment increases the number of whiskers interacting with cracks normal to their alignment direction, the crack-bridging mechanism is dominant for fracture toughness improvement (Fig. 8b).

4. Conclusions

Through investigation of R-curve behavior for the three materials with different whisker alignment, the following conclusions are obtained:

(1) The R-curve behavior of the three kinds of materials with different whisker alignment can be best described by using the improved exponential function, the results show that all the materials exhibit a well-defined R-curve behavior, which tends to become asymptotically flat with increasing crack length, and shows a higher threshold value corresponding with the point of the initial abrupt stable crack propagation.
(2) The results show that both tape casting and extrusion can considerably increase whisker alignment, and improve fracture toughness. The fracture toughness of material A, B and C are 11.18, 11.44 and 10.60 MPa $m^{1/2}$, and the corresponding threshold values with the stable crack propagation are 9.14, 10.92 and 9.32 MPa $m^{1/2}$, respectively.
(3) The results prove that whisker alignment is beneficial to improvement of fracture toughness, increase of critical crack length and crack tolerance. However, from tape casting to extrusion processing, an improved whisker alignment (material C) does not result in an expected fracture toughness increase.

Acknowledgment

The authors would like to thank Professor Z.D. Guan in Tsinghua University for his guidance during the R-curve measurement.

References

[1] K.T. Faber, A.G. Evans, Crack deflection process. I. Theory, Acta Metall. 31 (4) (1983) 565–576.
[2] P.F. Becher, Microstructural design of toughened ceramics, J. Am. Ceram. Soc. 74 (2) (1991) 255–269.
[3] D.-S. Park, M.-J. Choi, T.-W. Rod, H.-D. Kim, B.-D. Han, Orientation-dependent properties of silicon nitride with aligned reinforcing grains, J. Mater. Res. 15 (1) (2000) 130–135.
[4] M. Wu, G.L. Messing, Fabrication of oriented SiC-whisker-reinforced mullite matrix composite by tape casting, J. Am. Ceram. Soc. 77 (10) (1994) 2586–2592.
[5] K. Hirao, M. Ohashi, M.E. Brito, S. Kanzaki, Processing strategy for producing highly anisotropic silicon nitride, J. Am. Ceram. Soc. 78 (6) (1995) 1687–1690.
[6] Y. Goto, A. Tsuge, Mechanical properties of unidirectionally oriented SiC-whisker-reinforced Si_3N_4 fabricated by extrusion and hot-pressing, J. Am. Ceram. Soc. 76 (6) (1993) 1420–1424.
[7] D. Muscat, M.D. Pugh, R.A.L. Drew, Microstructure of an extruded β-silicon nitride whisker-reinforced silicon nitride composite, J. Am. Ceram. Soc. 75 (10) (1992) 2713–2718.
[8] N. Ramachandran, D.K. Shetty, Rising crack-growth-resistance (R-curve) behavior of toughened alumina and silicon nitride, J. Am. Ceram. Soc. 74 (10) (1991) 2634–2641.
[9] S.R. Choi, J.A. Salem, Crack-growth resistance of in situ-toughened silicon nitride, J. Am. Ceram. Soc. 77 (4) (1994) 1042–1046.
[10] C.-W. Li, D.-J. Lee, S.-C. Lui, R-curve behavior and strength for in-situ reinforced silicon nitrides with different microstructures, J. Am. Ceram. Soc. 75 (7) (1992) 1777–1785.
[11] C.-W. Li, J. Yamanis, Super-tough silicon nitride with R-curve behavior, Ceram. Eng. Sci. Proc. 10 (7–8) (1989) 632–645.
[12] R.F. Krause Jr., Rising fracture toughness from the bending strength of indented alumina beams, J. Am. Ceram. Soc. 71 (5) (1988) 338–343.
[13] S.K. Lee, D.K. Kim, C.H. Kim, Flaw-tolerance and R-curve behavior of liquid-phase-sintered silicon carbides with different microstructures, J. Am. Ceram. Soc. 78 (1) (1995) 65–70.
[14] R.F. Krause Jr., E.R. Ruller Jr., J.F. Rhodes, Fracture resistance behavior of silicon carbide whisker-reinforced alumina composites with different porosities, J. Am. Ceram. Soc. 73 (3) (1990) 559–566.
[15] H.-J. Choi, K.-S. Cho, J.-G. Lee, Y.-W. Kim, Silicon nitride–titanium nitride composites, J. Am. Ceram. Soc. 80 (10) (1997) 2681–2684.
[16] T. Ohji, K. Hirao, S. Kanzaki, Fracture resistance behavior of highly anisotropic silicon nitride, J. Am. Ceram. Soc. 78 (11) (1995) 3125–3128.
[17] J. Xi, Z.D. Guan, Investigation on characteristics of R-curve for engineering ceramics, in: Proceedings of the First China International Conference on High-Temperature Ceramics, 1998, pp. 73–76.
[18] B.R. Lawn, A.G. Evans, D.B. Marshall, Elastic/plastic indentation damage in ceramics: the median/radial crack system, J. Am. Ceram. Soc. 63 (9–10) (1980) 574–581.
[19] P. Chantikul, G.R. Antis, B.R. Lawn, D.D. Marshall, A critical evaluation of indentation techniques for measuring fracture toughness. II. Strength method, J. Am. Ceram. Soc. 64 (9) (1981) 539–543.
[20] G.R. Anstis, P. Chantikul, B.R. Lawn, D.B. Marshall, A critical evaluation of indentation techniques for measuring fracture toughness. I. Direct crack measurements, J. Am. Ceram. Soc. 64 (9) (1981) 533–538.
[21] M. Sakai, R.C. Bradt, Fracture toughness testing of brittle materials, Int. Mater. Rev. 38 (2) (1993) 53–78.
[22] J.C. Newman Jr., I.S. Raju, An empirical stress-intensity factor equation for the surface crack, Eng. Fract. Mech. 15 (1–2) (1981) 185–192.
[23] K. Ikeda, H. Igaki, Effect of surface flaw size on fracture strength of alumina ceramics, J. Am. Ceram. Soc. 70 (2) (1987) C29–C30.
[24] S.M. Smith, R.O. Scattergood, Crack-shape effects for indentation fracture toughness measurement, J. Am. Ceram. Soc. 75 (1992) 305–315.
[25] D.-S. Park, T.-W. Rod, B.-D. Han, H.-D. Kim, C. Park, J. Eur. Ceram. Soc. 22 (2002) 535–543.